Green Chemistry

PAPER

View Article Online
View Journal | View Issue

Cite this: *Green Chem.*, 2026, **28**, 1804

Development and systematic evaluation of aqueous triazole chloride-based deep eutectic solvents for efficient CO_2 capture

Qiangbing Shi, [a] Kaige Jia,[a] Xiangping Zhang, [b,c] Chuan Wang,[d] Paul Cobden, [d] Anna-Maria Beregi Amnéus,[e] David Muren[f] and Xiaoyan Ji *[a]

Deep eutectic solvents (DESs) have attracted considerable attention as promising alternatives to conventional solvents for mitigating CO_2 emissions due to their tunable structures, low volatility, and promising physicochemical properties. In this work, a series of [Triz]Cl/amine DESs were designed and synthesized and then formulated as 30 wt% aqueous solutions (30 wt% DES + 70 wt% H_2O) to systematically investigate how the type of hydrogen bond donor (HBD) affects their physicochemical properties, thermal stability, and CO_2 capture performance, and to identify the most effective solvent; their CO_2 absorption capacity, absorption rate, thermal stability, and desorption efficiency were determined experimentally, and a novel stepwise evaluation strategy was employed for identification. [Triz]Cl/DETA was identified, exhibiting significantly enhanced performance, with CO_2 absorption capacity, absorption rate, thermal stability, and cyclic loading increased by 34%, 12%, 114%, and 39%, respectively, when compared with the conventional monoethanolamine (MEA). Its viscosity (both before and after CO_2 absorption), oxidative stability, and corrosion resistance were further studied, confirming the superior performance, and the reaction mechanism was also elucidated. This work provides valuable insights into the structure–property relationships of DESs and establishes [Triz]Cl/DETA-based solvents as promising candidates for efficient and sustainable CO_2 capture applications.

Received 21st October 2025,
Accepted 11th December 2025

DOI: 10.1039/d5gc05611j

rsc.li/greenchem

Green foundation

1. We performed structure–function analysis for HBD in aqueous [TrizCl]-based DESs and identified [Triz]Cl/DETA that outperforms MEA while lowering volatility and corrosion, yielding design rules (optimization of amine density, flexibility, and H-bonding).
2. 30 wt% [Triz]Cl/DETA delivers 0.17 g-CO_2 per g-solvent, K_a = 0.183 min^{-1}, a desorption efficiency of 57% at 110 °C, and a cyclic loading of 0.09 g-CO_2 per g-solvent; the post-loading viscosity is ~7.5 mPa s. The corrosion rates are markedly lower than those of 30 wt% MEA (unloaded: 1.2×10^{-4} *vs.* 2.3×10^{-4} mm a^{-1}; loaded: 7.5×10^{-4} *vs.* 1.8×10^{-3} mm a^{-1}). No FTIR-detectable oxidation was observed after 5 h of O_2.
3. Regeneration temperature/energy (target ≤100 °C) *via* composition tuning is reduced; durability (extension of O_2 exposure beyond 5 h) is verified; and corrosion is optimized by optimizing the DES–water ratio and materials selection, while quantifying solvent loss relative to that of MEA.

1. Introduction

The combustion of fossil fuels has driven industrial modernization but has also produced unprecedented anthropogenic CO_2 emissions.[1] The concentration of CO_2 in the atmosphere has continued to rise and reached 422.5 ppm in 2024,[2] the first year on record with a global average temperature about 1.5 °C above pre-industrial levels.[3] It has been observed that the global per capita CO_2 emissions and the global mean temperature have risen substantially since the 19th century, demonstrating a clear positive correlation. Therefore, CO_2 mitigation and removal have become critical scientific and technological concerns for achieving global climate goals and maintaining climate stability.[4]

To mitigate these challenges, carbon capture, utilization, and storage (CCUS)[5] has been considered indispensable, owing to its application in large-scale industrial operation. Within the CCUS chain, CO_2 capture serves as a critical com-

[a]*Energy Engineering, Department of Engineering Science and Mathematics, Luleå University of Technology, Luleå 97187, Sweden. E-mail: xiaoyan.ji@ltu.se*
[b]*State Key Laboratory of Heavy Oil Processing, College of Chemical Engineering and Environment, China University of Petroleum, Beijing, 102249, China*
[c]*Center of Ionic Liquids and Green Energy, Beijing Key Laboratory of Solid State Battery and Energy Storage Process, Institute of Process Engineering, Chinese Academy of Sciences, Beijing, 100190, China*
[d]*Swerim AB, Luleå 97125, Sweden*
[e]*SMA Mineral AB, Filipstad 68227, Sweden*
[f]*Linde Gas AB, Luleå 97188, Sweden*

ponent, making the development of efficient CO_2 capture paramount. Among the available technologies for CO_2 capture, chemical-based absorption is widely regarded as the most promising one, due to its high selectivity, large absorption capacity, technological maturity, and flexibility for integration with existing industrial systems. For the chemical absorption routes, amine-based solvents, such as monoethanolamine (MEA), diethanolamine (DEA), methyl diethanolamine (MDEA), and their blends, are the most widely employed in research and industrial practice.[5] Among the studied amines, primary and secondary amines (*e.g.*, MEA and DEA) provide high absorption capacities and fast CO_2 capture, but their use is often constrained by volatility, corrosivity, and high regeneration energy demand; tertiary amines (*e.g.*, MDEA) exhibit lower volatility and reduced corrosivity, but their inherently low CO_2 absorption rates remain a significant drawback.[6] Hence, the development of alternative absorbents remains imperative to overcome the limitations of conventional systems.

Ionic liquids (ILs) exhibit exceptional properties, including high thermal stability, negligible volatility, and tunable structures, making them highly adaptable for diverse applications.[7] Nevertheless, the high production cost of conventional ILs remains a critical barrier to their large-scale deployment. Deep eutectic solvents (DESs) are a distinct class of IL analogues composed of a hydrogen bond donor (HBD) and a hydrogen bond acceptor (HBA).[8] DESs not only retain many of the advantageous properties of ILs but also offer additional benefits, such as low cost and biocompatibility. Development of DESs has become more prominent than that of conventional ILs in recent years.

To develop DESs as absorbents for CO_2 capture, recent studies have highlighted that the choice of HBD is decisive.[9] For instance, Jiang *et al.*[10] showed that employing acylamido compounds as HBDs led to notably high capacities, and 1,5-diazabicyclo[4.3.0]non-5-ene (DBN)/2-imidazolidone (EU) (2 : 1) reached 0.23 g-CO_2 per g-solvent at 45 °C and 1 bar, attributed to multiple N-site interactions that enhance chemisorption. Likewise, within a chloride–amine family using a fixed HBA ([MEA]Cl), replacing the HBD from MEA to ethylenediamine (EDA) markedly increased the capacity, where [MEA]Cl/EDA achieved ~0.30 g-CO_2 per g-solvent under ambient pressure.[11] With choline chloride as the HBA, switching the HBD from urea to ethylene glycol reduces viscosity but also weakens chemisorption strength and decreases equilibrium loading, revealing a rate–capacity trade-off controlled by the HBD identity.[12] Similarly, the superbase 1,1,3,3-tetramethylguanidine (TMG) was used as the HBA and paired with polyol HBDs (*e.g.*, glycerol and ethylene glycol) to tune both the absorption kinetics and the energy required for desorption *via* shifting the dominant binding pathway (from carbamate to bicarbonate under humid conditions).[13]

Despite growing evidence highlighting the importance of the HBD component for the performance of DESs, previous research[14] has encountered three primary challenges. First, the formulation space was only partially investigated by focusing on EDA as the HBD and varying the types of HBAs, thus leaving the vast spectrum of potential HBDs largely unexplored. Second, the EDA-based DESs demonstrated only moderate thermal stability, surpassing that of MEA, but still inadequate at relatively high temperatures and with extended cycling. Third, crucial durability indicators relevant to practical applications, such as oxidative stability, corrosion resistance, and cyclic stability, have not been systematically evaluated or sufficiently considered.

Additionally, for the DESs with outstanding CO_2 capture capacities, it is common for a sharp viscosity rise to occur following the CO_2 absorption, which has frequently been overlooked.[15,16] For example, neat [MEA]Cl/MDEA shows a multi-fold viscosity increase (from 275 to 1500 mPa s) upon CO_2 loading, which severely suppresses mass transfer and lowers the absorption rate.[17] To address this issue, water, an inexpensive and environmentally benign cosolvent, is highly effective at adjusting viscosity. For example, a 40 wt% [MEA]Cl/EDA + 60 wt% H_2O solution maintained a low viscosity both before and after CO_2 absorption (4.4 and 13.3 mPa s at 25 °C, respectively).[18] Similarly, a [Ch]Cl/MEA solution containing 75 vol% H_2O exhibited a high CO_2 absorption capacity of 0.19 g-CO_2 per g-solvent and low viscosity (2.2 mPa s) at 20 °C and 1.5 MPa.[19]

To address the research gaps and given prior evidence that 1,2,4-triazolium chloride ([Triz]Cl) demonstrates favorable CO_2 absorption/desorption efficiency and thermal stability, in this work, a series of [Triz]Cl-based DESs was designed and synthesized by pairing [Triz]Cl with structurally varied amine HBDs and then mixing with water as a cosolvent to form aqueous solutions. A stepwise method was used to identify promising DESs based on the CO_2 absorption capacity, absorption rate, thermal stability, and cyclic loading under identical conditions. The most effective DES was subsequently subjected to application-relevant evaluations, including viscosity measurements before and after CO_2 absorption, oxidative stability testing, corrosion compatibility assessment, and mechanistic analysis of the CO_2 capture. Through this approach, a practical design and screening strategy was developed to identify DESs as absorbents for CO_2 capture, and guidance directly relevant to industrial CO_2 capture deployment was provided.

2. Experimental

2.1. Materials

CO_2 (99.99%), 1,2,4-triazole (Triz, Macklin, 99%, CAS no. 288-88-0), hydrochloric acid (HCl, 37%, Macklin, CAS no. 7647-01-0), ethylenediamine (EDA, Lingfeng, 99.5%, CAS no. 107-15-3), diethylenetriamine (DETA, Macklin, 99%, CAS no. 111-40-0), tetraethylenepentamine (TEPA, Macklin, 95%, CAS no. 112-57-2), *N*-methyldiethanolamine (MDEA, Macklin, 98%, CAS no. 105-59-5), diethanolamine (DEA, Macklin, 99%, CAS no. 111-42-2), monoethanolamine (MEA, Macklin, 99%, CAS no. 141-43-5), 2-amino-2-methyl-propanol (AMP, Sigma-Aldrich, >95%, CAS no. 124-68-5) and aminoethylethanolamine (AEEA, Macklin, 99%, CAS no. 111-41-1) were used in this study. The structures of all studied HBDs are shown in Table 1.

Table 1 Molecular characteristics and amine-group density of the selected HBDs

HBD	Molar mass (g mol^{-1})	Molecular structure	Number of amine groups	Molar amine density (mol g^{-1})
Ethylenediamine (EDA)	60.10		2	0.033
Diethylenetriamine (DETA)	103.17	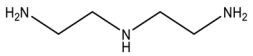	3	0.029
Tetraethylenepentamine (TEPA)	189.3	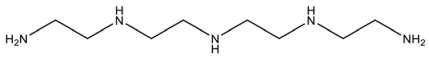	5	0.026
2-Amino-2-methyl-propanol (AMP)	89.14	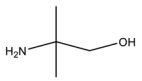	1	0.011
Aminoethylethanolamine (AEEA)	104.15	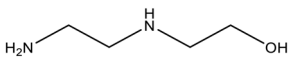	2	0.019
Monoethanolamine (MEA)	61.08	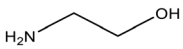	1	0.016
Diethanolamine (DEA)	105.14	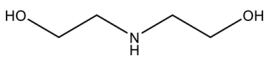	1	0.010
N-Methyldiethanolamine (MDEA)	119.16	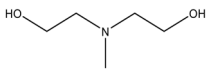	1	0.008

2.2. Preparation of DESs

The HBA, [Triz]Cl, was synthesized *via* a one-step anion-exchange method. During the synthesis, equimolar HCl was added dropwise into a round-bottom flask containing an aqueous 1,2,4-triazole solution, under stirring in an ice bath (1 °C) to minimize HCl volatilization. Afterward, the mixture was stirred at room temperature for 3 hours, followed by rotary evaporation at 60 °C and vacuum drying at the same temperature for 3 hours to remove excess water. To eliminate the remaining impurities, the sample was then connected to an ultra-high vacuum pump at 70 °C, yielding white crystalline [Triz]Cl. The DES, for example, [Triz]Cl/DETA, was prepared by mixing [Triz]Cl with DETA at a molar ratio of 1 : 5, followed by stirring at 60 °C for 3–5 hours to obtain a clear and homogeneous solvent. Subsequently, [Triz]Cl/DETA was diluted with H_2O at a mass ratio of 3 : 7 to produce the aqueous [Triz]Cl/DETA solution for CO_2 capture. Other aqueous DES solutions were prepared following the same procedure.

2.3. Characterization

^{13}C NMR spectra were measured using a 60 MHz NMR spectrometer (Spinsolve 60). Fourier Transform Infrared (FTIR, Nicolet 8700) spectroscopy was employed to identify functional groups of samples in the range of 400–4000 cm^{-1} with a resolution of 4 cm^{-1}. Thermal stability was evaluated *via* thermogravimetric analysis (TGA) using a TA SDT650 instrument, with DES samples heated from room temperature to 400 °C at a rate of 10 °C min^{-1} under an N_2 flow of 60 mL min^{-1}. Viscosity measurements of the solvents before and after CO_2 absorption were performed at 25 °C using an Anton Paar 2000 ME viscometer (accuracy ±0.35%). Oxidative stability was evaluated by comparing FTIR spectra recorded before and after 5 h of exposure to O_2 and N_2.

2.4. CO_2 absorption capacity and rate

The CO_2 absorption capacity was measured using a gravimetric method,[18] following the procedure described in our previous work, as shown in Fig. S1.[14] Briefly, about 7 g of solvent was placed in a 15 mL gas absorption tube, which was immersed in a water bath maintained at a constant temperature. CO_2 gas was then bubbled into the solvent under atmospheric pressure at a flow rate of 60 mL min^{-1}, controlled by a mass flow controller (YJ-700C). The entire gas absorption tube was weighed at regular intervals using an electronic analytical balance with an accuracy of ±0.1 mg. Absorption equilibrium was reached when there was no further increase in mass. Each experiment was repeated at least twice, and the average value was reported with an uncertainty of ±0.01 g-CO_2 per g-solvent. Before conducting experiments on the systems studied in this work, a 30 wt% MEA aqueous solution was investigated to ensure experimental reliability and accuracy, and a 30 wt% [Triz]Cl/EDA aqueous solution was also tested as a representative DES. Details of the uncertainty analysis and the corresponding raw data are provided in Fig. S2 of the SI.

The kinetics of the CO_2 capture process were analyzed, where the instantaneous CO_2 absorption rate (r_t, g-CO_2 per (g-solvent min)) and the apparent absorption rate constant (K_a, min^{-1}) were calculated based on formulas derived from previous studies,[20] as shown below:

$$r_t = \frac{dn_t}{dt} \quad (1)$$

$$n_t = n_e(1 - e^{-K_a t}) \quad (2)$$

where n_t is the CO_2 capacity (g-CO_2 per g-solvent) at time t and n_e is the saturated CO_2 capacity. The value of K_a was obtained by fitting the experimental data.

2.5. Solvent regeneration

The solvent regeneration process was conducted in a three-neck flask containing CO_2-saturated DES, which was heated to 110 °C in an oil bath and continuously stirred at 150 rpm, as shown in Fig. S1. To recover water vapor released alongside CO_2, the gas stream was passed through a serpentine condenser maintained at 1 °C, followed by concentrated sulfuric acid to remove residual moisture.[21] The desorption rate (r_d, g-CO_2 per (g-solvent min)) was obtained from eqn (3), and then the CO_2 cyclic loading (n_d) was obtained from the integral of r_d over time as shown in eqn (4). The CO_2 desorption efficiency (η) was calculated from the cyclic loading and the saturated CO_2 capacity n_e as expressed in eqn (5):

$$r_d = \frac{Q_t \times M_{CO_2}}{m_s \times 22.4 \times 1000}\left(\frac{P \times (T_0 + 273.15)}{P_0 \times (T + 273.15)}\right) \quad (3)$$

$$n_d = \int_0^t r_d \mathrm{d}t \quad (4)$$

$$\eta = \frac{n_d}{n_e} \times 100\% \quad (5)$$

where Q_t is the CO_2 flow rate at the outlet of the round-bottom flask (m^3 min^{-1}); M_{CO_2} is the molar mass of CO_2; P and T are the experimental pressure and temperature (kPa and °C); P_0 and T_0 are the standard pressure (101.325 kPa) and standard temperature (0 °C), respectively; and m_s is the solvent mass.

2.6. Corrosion analysis

To study the corrosive effects of the absorbents on steel, a three-electrode electrochemical system was used.[22] The setup consists of a 20# carbon steel working electrode (W.E.), an Ag/AgCl (saturated KCl) reference electrode (R.E.), and a platinum counter electrode (C.E.). Before testing, the steel samples were cleaned with acetone and ethanol. Electrochemical measurements were performed using a CHI760E Electrochemical Workstation. Each specimen was stabilized at the open-circuit potential (OCP). Tafel polarization was recorded by scanning from −100 to +100 mV *versus* OCP at a rate of 10 mV s^{-1}. The corrosion current density (i_{corr}) was obtained by Tafel extrapolation, and the corrosion rate (CR, mm a^{-1}) was calculated as

$$CR = \frac{3.27 \times 10^{-3} \times i_{corr} \times w}{A \times \rho} \quad (6)$$

where w is the equivalent weight of 20# carbon steel (g $equiv.^{-1}$); A is the exposed surface area (cm^2); and ρ is the density of 20# carbon steel (g cm^{-3}).

3. Results and discussion

3.1. Structural and functional features of HBDs

HBDs play a critical role in the CO_2 capture performance of DESs, with representative examples and their corresponding absorption capacities summarized in Table 2. Depending on their functional groups, HBDs can participate in different types of hydrogen-bonding and CO_2 interaction mechanisms. The most studied classes include acylamides, polyols, carboxylic acids, alkanolamines, and polyamines. Acylamido-based HBDs, such as urea, contain both carbonyl (C═O) and amino (–NH_2) groups, which form strong hydrogen bonds with HBAs, significantly lowering the eutectic temperature.[23] Moreover, as shown in Fig. 1(a), their amine groups can chemically interact with CO_2 to form carbamate-like intermediates, enhancing CO_2 capture efficiency.[10] However, the relatively high volatility and limited chemical stability of some acyla-

Table 2 CO_2 absorption performance of DESs based on different types of HBDs

HBD type	DESs (molar ratio)	HBD	T (K)/P (bar)	Capacity (g-CO_2 per g-solvent)	Ref.
Acylamido compounds	[Ch]Cl/urea (1 : 2)	Urea	313.15/123.4	0.04	23
	DBN/DMU (2 : 1)	Dimethylolurea (DMU)	318.15/1.0	0.04	10
	DBN/DMLU (2 : 1)	1,3-Dimethylurea (DMLU)	318.15/1.0	0.17	
	DBN/EU (2 : 1)	2-Imidazolidone (EU)	318.15/1.0	0.23	
	DBN/EU (3 : 1)	2-Imidazolidone (EU)	318.15/1.0	0.19	
Polyols	[TETA]Cl/DEG (1 : 2)	Diethylene glycol (DEG)	313.15/1.0	0.16	25
	[TETA]Cl/EG (1 : 3)	Ethylene glycol (EG)	313.15/1.0	0.18	
	[N_{2222}]Triz/EG (1 : 2)	Ethylene glycol (EG)	298.15/1.0	0.13	26
	[N_{2222}]Im/EG (1 : 2)	Ethylene glycol (EG)	298.15/1.0	0.13	
	[Ch]Cl/Gly (1 : 1)	Glycerol (Gly)	298.2/1.0	0.02	31
Carboxylic acids	[BHDE]Cl/L (1 : 2)	Lactic acid (L)	298.15/2.8	0.001	27
	[BHDE]Cl/Ac (1 : 2)	Acetic acid (Ac)	298.15/2.1	0.003	
	[N_{4444}]Cl/DECA (1 : 2)	Decanoic acid (DECA)	308.15/0.9	0.002	28
	[N_{8881}]Cl/DECA (1 : 2)	Decanoic acid (DECA)	323.15/0.9	0.002	
	[N_{8888}]Cl/DECA (1 : 2)	Decanoic acid (DECA)	323.15/0.9	0.002	
Alcohol amine	[TEPA]Cl/MEA (1 : 2)	Monoethanolamine (MEA)	298.15/1.0	0.41	9
	[DEA]Cl/MDEA (1 : 3)	Methyldiethanolamine (MDEA)	298.15/1.0	0.11	17
	[MDEA]Cl/MDEA (1 : 3)	Methyldiethanolamine (MDEA)	298.15/1.0	0.06	
Polyamine	[MEA]Cl/EDA (1 : 4)	Ethylenediamine (EDA)	328.15/1.0	0.36	29
	[MEA]Cl/DETA (1 : 3)	Diethyltriamine (DETA)	313.15/1.0	0.18	30
	[MEA]Cl/TETA (1 : 3)	Triethylenetetramine (TETA)	313.15/1.0	0.17	
	[MEA]Cl/TEPA (1 : 3)	Tetraethylenepentamine (TETA)	313.15/1.0	0.10	

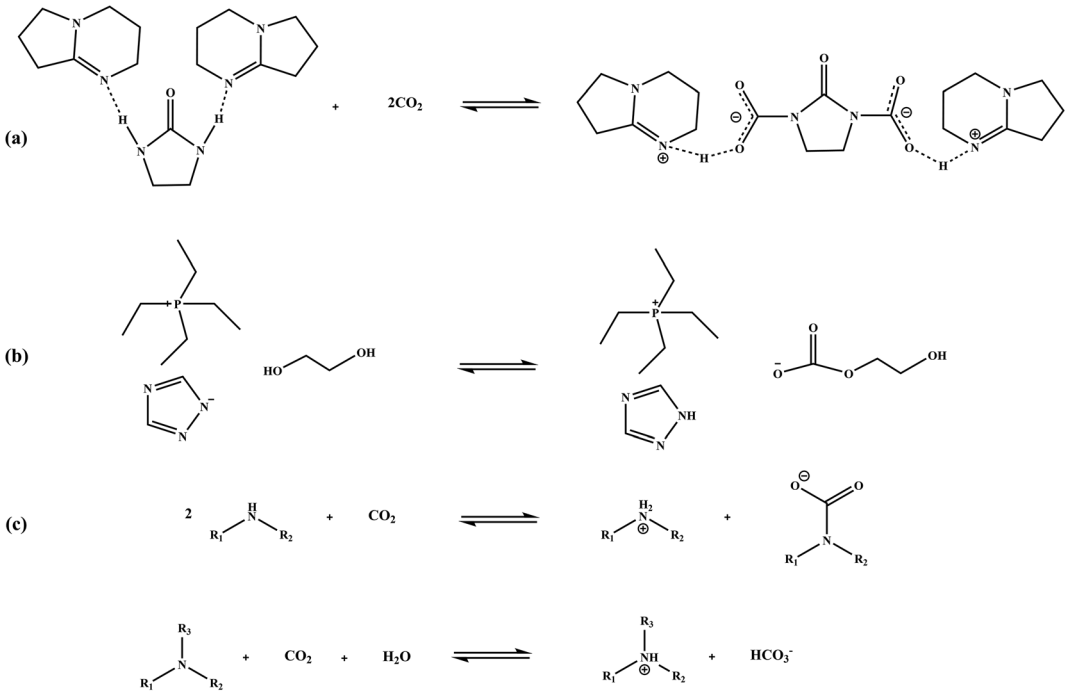

Fig. 1 Representative CO_2 capture pathways involving different HBD types in DESs: (a) acylamide, (b) polyol, and (c) amine.

mides under regeneration conditions constrain their large-scale applicability.

Polyol-based HBDs, such as ethylene glycol (EG) and glycerol, contain multiple hydroxyl (–OH) groups, which facilitate extensive hydrogen-bonding networks with HBAs, thereby promoting CO_2 absorption physically and chemically.[24] For example, when using EG and diethylene glycol (DG) as HBDs, and triethylenetetramine chloride ([TETA]Cl) as the HBA to prepare various DESs, it is found that EG or DG can activate the –NH– and $–NH_2$ groups in [TETA]Cl, thereby improving the basicity of the DESs and enhancing CO_2 capacity.[25] FTIR and NMR analyses have demonstrated that EG can chemically react with CO_2 to produce carbonate species, facilitated by activation of its hydroxyl oxygen through interaction with the cationic HBA (Fig. 1b).[26] In addition, polyol-based DESs exhibit high thermal stability and low volatility, which is beneficial for solvent regeneration and long-term stability.

Carboxylic acid-based HBDs can be categorized into hydrophilic and hydrophobic types, both primarily capturing CO_2 through physical absorption.[27] Hydrophilic acids (*e.g.*, lactic acid and formic acid) form dense hydrogen bonding networks *via* their –COOH groups, depressing melting points and increasing polarity to enhance CO_2 solubility. In contrast, hydrophobic acids (*e.g.*, dodecanoic acid) yield less polar DESs that demonstrate superior thermal stability and require lower energy for solvent regeneration.[28]

Amino alcohols and polyamines are among the most promising HBD families owing to their low cost, high reactivity toward CO_2, and favorable physicochemical characteristics.[17] Amino alcohols possess both amine ($–NH_2$) and hydroxyl (–OH) groups, offering dual sites for hydrogen bonding and CO_2 activation,[9] while polyamines are rich in multiple nucleophilic amine sites, capable of forming strong hydrogen bonding networks with HBAs.[29] These features enable the formation of stable and dense hydrogen bonding networks with HBAs, thereby facilitating the self-assembly of low-melting-point DESs and providing abundant reactive sites for CO_2 interaction.[30] As depicted in Fig. 1(c), primary and secondary amines react directly with CO_2 to form carbamate species, while tertiary amines facilitate CO_2 hydration to produce bicarbonate ions in aqueous media. This chemical versatility enables amine-based DESs to achieve high absorption capacities and fast kinetics compared with other HBD types.

As summarized in Table 2, DESs incorporating amine-based HBDs consistently exhibit superior CO_2 absorption capacities. Therefore, in this work, amine-based HBDs were selected to systematically investigate the structure–property relationships. More specifically, EDA, DETA, TEPA, MEA, DEA, MDEA, AMP, and AEEA were chosen, which encompass a broad range of molecular architectures, from polyamines to alkanolamines and tertiary amines, enabling a systematic comparison of how the number of amine groups, steric hindrance, and hydroxyl substitution influence CO_2 absorption capacity, kinetics, and thermal stability.

3.2. Absorption performance of aqueous DESs

Based on the findings in section 3.1, eight amines with potentially superior CO_2 absorption capacities were selected as the HBDs for this study. For a DES solution, the ratio of HBA to HBD and the content of water will also influence the pro-

perties and performance. Previously, Shukla *et al.*[32] systematically investigated the properties of [Im]Cl/EDA at various HBA : HBD molar ratios (1 : 4, 1 : 5, and 1 : 6). The results showed that although [Im]Cl/EDA (1 : 5) exhibited a slightly lower CO_2 absorption capacity than [Im]Cl/EDA (1 : 6), its thermal degradation was significantly lower than that of the 1 : 4 and 1 : 6 counterparts. Additionally, the viscosity of the 30 wt% [Im]Cl/EDA (1 : 5) aqueous solution was found to be below 5 mPa s. Therefore, a 30 wt% DES aqueous solution with an HBA : HBD molar ratio of 1 : 5 was prepared for all the studied DESs in this work to reflect practical application scenarios.

Table 3 CO_2 absorption data of 30 wt% DES aqueous solutions

DESs	CO_2 absorption capacity (g-CO_2 per g-solvent)	Instantaneous rate (g-CO_2 per (g-solvent min))	Apparent rate constant K_a (min^{-1})
[Triz]Cl/EDA	0.18	0.025	0.20
[Triz]Cl/DETA	0.17	0.024	0.18
[Triz]Cl/AMP	0.10	0.013	0.12
[Triz]Cl/AEEA	0.09	0.011	0.15
[Triz]Cl/MDEA	0.04	0.001	0.03
[Triz]Cl/MEA	0.08	0.011	0.14
[Triz]Cl/TEPA	0.13	0.010	0.09
[Triz]Cl/DEA	0.05	0.007	0.15

3.2.1. Absorption capacity. To elucidate the effect of HBD on the CO_2 absorption capacity, dynamic CO_2 absorption curves were measured over time. The results are shown in Table 3. For the DESs based on polyamine HBDs, aqueous [Triz]Cl/EDA, [Triz]Cl/DETA, and [Triz]Cl/TEPA solutions achieved the top 3 capacities of 0.18, 0.17, and 0.13 g-CO_2 per g-solvent, respectively, as shown in Fig. 2(a). For the alkanolamine-based DESs, [Triz]Cl/AMP (0.10 g-CO_2 per g-solvent) and [Triz]Cl/AEEA (0.09 g-CO_2 per g-solvent) exhibited relatively higher CO_2 absorption capacities than [Triz]Cl/MEA (0.08 g-CO_2 per g-solvent), [Triz]Cl/DEA (0.05 g-CO_2 per g-solvent), and [Triz]Cl/MDEA (0.04 g-CO_2 per g-solvent). This order corresponds to their molar amine group densities (except for [Triz]Cl/AMP), as shown in Table 3 and Fig. S3(a), indicating that higher amine group densities provide more reactive sites for CO_2 capture, thereby enhancing the absorption performance of DESs, such as [Triz]Cl/EDA. However, the relatively high CO_2 absorption capacity of [Triz]Cl/AMP, despite its low amine group density, may be attributed to the unique structure of AMP, where the structural synergy and

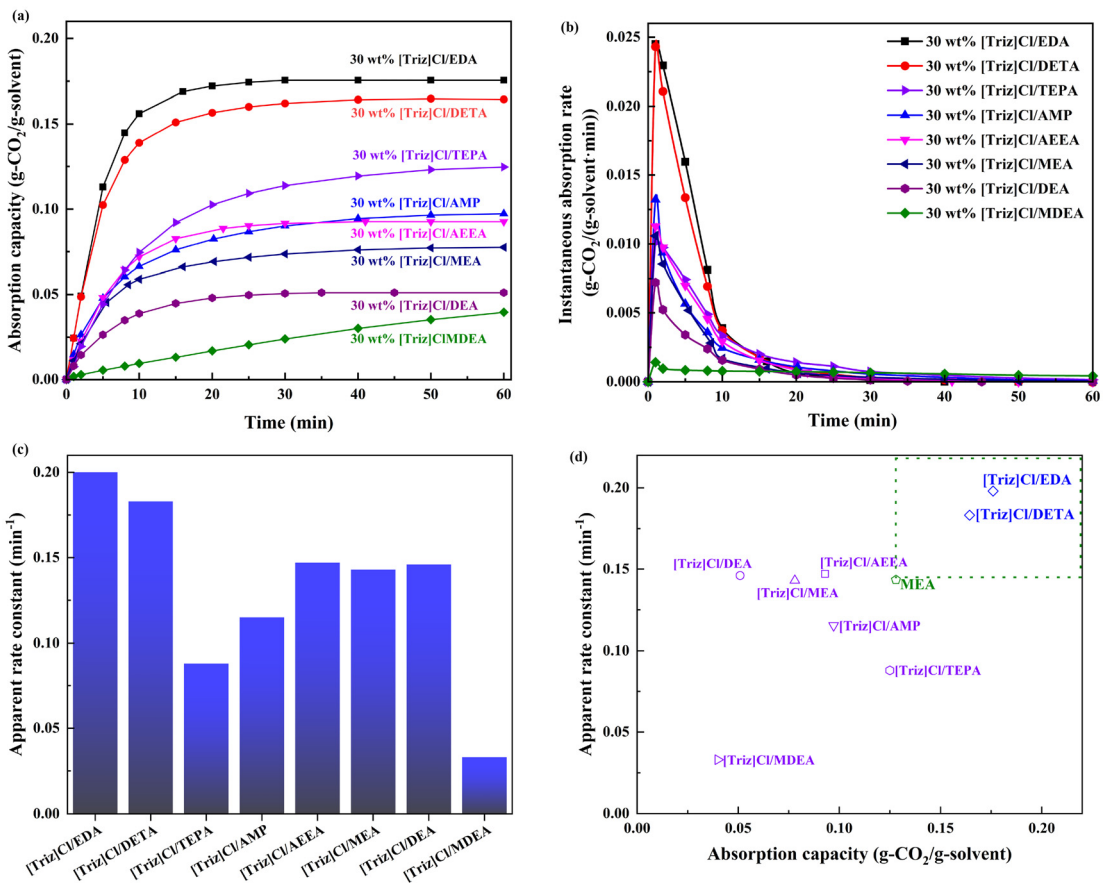

Fig. 2 (a) CO_2 absorption curves, (b) instantaneous CO_2 absorption rate curves, (c) apparent rate constant, and (d) systematic comparison of CO_2 absorption capacity and apparent rate constant of aqueous DES solutions at 22 °C and 1 bar.

possible weak interactions between the hydroxyl group and CO_2 together enhance CO_2 solubility.[33] Moreover, the DESs incorporating polyamine-based HBDs exhibited significantly higher CO_2 absorption capacities compared to those with alkanolamine-based HBDs. Notably, [Triz]Cl/MEA exhibited a higher CO_2 absorption capacity than [Triz]Cl/DEA, indicating that primary amines possess stronger CO_2 binding ability than secondary amines. [Triz]Cl/MDEA showed the lowest capacity, consistent with the typical trend of primary > secondary > tertiary amines.[34]

3.2.2. Absorption kinetics. The instantaneous CO_2 absorption rates (r_t) of DESs with different HBDs, alongside the corresponding apparent absorption rate constants (K_a), were calculated by fitting the experimental data using eqn (1) and (2), with the results summarized in Table 3. As shown in Fig. 2(b), all DESs exhibited a characteristic two-stage absorption profile. In the initial 1–5 minutes, the instantaneous absorption rate increased rapidly due to the presence of abundant free active sites. Subsequently, the rate declined gradually, as saturation and diffusion limitations became dominant, requiring CO_2 molecules to diffuse deeper into the DES matrix to access the remaining reactive sites. Among all the DESs, [Triz]Cl/EDA and [Triz]Cl/DETA demonstrated the highest instantaneous CO_2 absorption rates (~0.025 and 0.024 g-CO_2 per (g-solvent min)), indicating rapid early-stage chemisorption. These were followed, in descending order, by [Triz]Cl/AMP, [Triz]Cl/AEEA, [Triz]Cl/MEA, [Triz]Cl/TEPA, [Triz]Cl/DEA, and [Triz]Cl/MDEA. However, it is noteworthy that the ranking of apparent rate constants does not fully match that of the instantaneous absorption rates, as shown in Fig. 2(c). For instance, [Triz]Cl/TEPA has a lower apparent rate constant than [Triz]Cl/DEA, but a higher instantaneous absorption rate. This discrepancy is expected, as the former reflects early stage chemisorption kinetics, while the latter accounts for the overall absorption process, including mass transfer and diffusion limitations.[35] Therefore, both parameters are complementary and should be considered jointly when evaluating DES performance for CO_2 capture.

To comprehensively compare the CO_2 absorption capacity and apparent rate constant of aqueous DESs with different HBDs, as well as to compare their performance relative to conventional MEA, the absorption performance data of all tested DESs are summarized in Fig. 2(d). The data demonstrate that [Triz]Cl/EDA and [Triz]Cl/DETA exhibit significantly superior performance in both CO_2 absorption capacity and apparent absorption rate constant compared to the other DESs and MEA. This may be attributed to their higher amine density and the lower steric hindrance. These findings highlight the critical role of HBD selection in optimizing CO_2 capture performance.

3.3. Thermal stability of DESs

As illustrated in Fig. 3, the thermal stability of [Triz]Cl-based DESs (neat, water-free samples) was evaluated using thermogravimetric analysis (TGA) and differential thermogravimetry (DTG). The onset temperature (T_{onset}) and the peak temperature (T_{peak}) were used to quantitatively evaluate the thermal stability of the DESs. T_{onset} is defined as the temperature at which the weight baseline intersects the tangent of the TGA curve, corresponding to the beginning of thermal decomposition, as shown in Fig. S4. In contrast, T_{peak} represents the temperature at which the sample exhibits the maximum decomposition rate and corresponds to the peak in the DTG curve.

The results show that all DESs exhibit higher thermal stability than pure MEA (Table 4), confirming that DES formation enhances solvent stability. Specifically, MEA exhibited the lowest stability, with a T_{onset} of 83 °C and a T_{peak} of only 110 °C. Among the samples, [Triz]Cl/TEPA demonstrated the highest T_{onset} (261 °C) and T_{peak} (295 °C), alongside minimal weight loss (0.7% at 110 °C). This superior stability is attributed to the high molecular complexity of TEPA, which facilitates the formation of extensive hydrogen-bonding networks with the HBA, thereby enhancing the structural integrity of the DES. In contrast, [Triz]Cl/EDA displayed the lowest thermal stability among the polyamine-based DESs, with a T_{onset} of only 90 °C and a substantial weight loss of 23%. This stark difference is primarily due to the low molecular weight and

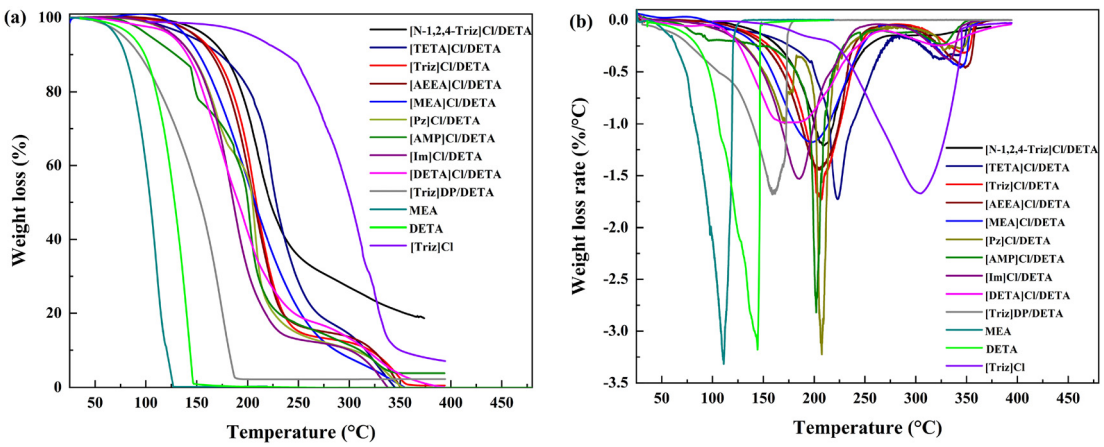

Fig. 3 (a) TGA and (b) DTG curves of pure DESs with different HBDs, compared with MEA, DETA, and [Triz]Cl.

Table 4 Thermal stability of pure [Triz]Cl-based DESs, MEA, DETA, and [Triz]Cl

DES	T_{onset} (°C)	T_{peak} (°C)	Weight loss at 110 °C (%)
[Triz]Cl/EDA	90	109	23.0
[Triz]Cl/DETA	178	207	0.7
[Triz]Cl/TEPA	261	295	0.7
[Triz]Cl/MEA	155	186	1.6
[Triz]Cl/DEA	172	259	1.1
[Triz]Cl/MDEA	199	247	0.7
[Triz]Cl/AEEA	224	247	0.2
[Triz]Cl/AMP	160	171	5.7
MEA	83	110	40.0
DETA	101	141	13.5
[Triz]Cl	255	304	0.1

boiling point of EDA, resulting in high volatility and increased susceptibility to thermal degradation. [Triz]Cl/DETA, on the other hand, exhibited intermediate stability, with a T_{onset} of 178 °C, a T_{peak} of 207 °C, and negligible weight loss (0.7%), reflecting a balance between molecular complexity and volatility. [Triz]Cl/MDEA and [Triz]Cl/AEEA exhibited relatively high T_{onset} values of 199 °C and 224 °C, respectively, along with low weight losses (0.7% and 0.2%), indicating favorable thermal resilience. In contrast, [Triz]Cl/MEA and [Triz]Cl/AMP showed relatively low T_{onset} temperatures (155 °C and 160 °C, respectively) and higher weight losses (1.6% and 5.7%).

Overall, the thermal stability of DESs followed the trend: [Triz]Cl/TEPA > [Triz]Cl/AEEA > [Triz]Cl/MDEA > [Triz]Cl/DETA > [Triz]Cl/DEA > [Triz]Cl/AMP > [Triz]Cl/MEA > [Triz]Cl/EDA > MEA. These findings highlight that the thermal stability of DESs is predominantly governed by the physical properties and structural characteristics of the HBD, as well as the strength of hydrogen bonding between the HBD and HBA. For further analysis, Fig. S3(b) shows that the T_{onset} and T_{peak} of the DESs increase with the boiling point of the HBD. DESs based on higher-boiling, higher-molecular-weight HBDs (*e.g.*, TEPA, AEEA, and MDEA) are more thermally stable than those using the lower-boiling HBDs (*e.g.*, MEA and EDA). This suggests that stronger hydrogen-bonding networks and less volatile HBDs enhance the intrinsic thermal stability of the DESs.

3.4. First-step screening and desorption performance of aqueous DESs

As illustrated in Fig. 2(d), 30 wt% [Triz]Cl/EDA and [Triz]Cl/DETA demonstrate significantly superior CO_2 capture performance, exhibiting higher absorption capacities (0.18–0.17 g-CO_2 per g-solvent) and faster absorption rate constants (0.20–0.18 min^{-1}) compared to other 30 wt% DES aqueous solutions (0.05–0.13 g-CO_2 per g-solvent; 0.03–0.15 min^{-1}) and 30 wt% MEA (0.12 g-CO_2 per g-solvent; 0.16 min^{-1}). These distinctive advantages have qualified 30 wt% [Triz]Cl/EDA and [Triz]Cl/DETA as primary candidates for subsequent investigations. Meanwhile, thermal stability analysis revealed that pure [Triz]Cl/TEPA and [Triz]Cl/AEEA possess exceptional thermal resistance with high T_{onset} values of 261 °C and 224 °C, respectively, ranking highest among all the evaluated DESs. However, [Triz]Cl/TEPA exhibited suboptimal absorption kinetics (0.09 min^{-1}), rendering it industrially impractical. In contrast, although [Triz]Cl/AEEA exhibited a lower CO_2 absorption capacity and rate constant (0.09 g-CO_2 per g-solvent and 0.15 min^{-1}) than MEA, its outstanding thermal stability (T_{onset} = 224 °C, 0.2 wt% weight loss at 110 °C) made it a more promising candidate. Therefore, [Triz]Cl/AEEA was selected as the third potential absorbent, alongside [Triz]Cl/EDA and [Triz]Cl/DETA, for further study (Fig. 4).

As a key step in the absorption–desorption cycle, CO_2 desorption is equally vital as absorption, as it governs the overall energy efficiency and long-term sustainability of the process. In this work, desorption at 110 °C was identified as the optimal condition, providing a favorable balance between the amount of CO_2 desorbed and the desorption rate, as shown in Fig. S5. To this end, the desorption performance of the CO_2-saturated aqueous DES solutions was evaluated by measuring the time-dependent CO_2 desorption rate, desorption efficiency, and cyclic loading. As shown in Fig. 5(a), the peak desorption rates of [Triz]Cl/DETA, [Triz]Cl/EDA, [Triz]Cl/AEEA, and MEA are 0.011, 0.013, 0.009, and 0.009 g-CO_2 per (g-solvent min), respectively. In comparison, [Triz]Cl/EDA and [Triz]Cl/DETA exhibited desorption rates 44% and 22% higher than that of MEA, respectively, whereas [Triz]Cl/AEEA showed a similar desorption rate to MEA. Furthermore, as shown in Fig. 5(b), the desorption efficiencies of [Triz]Cl/DETA, [Triz]Cl/EDA, [Triz]Cl/AEEA, and MEA are 57%, 46%, 56%, and 57%, respectively. Correspondingly, their CO_2 cyclic loadings, presented in Fig. 5(c), are 0.09, 0.08, 0.05, and 0.07 g-CO_2 per g-solvent, respectively. As a result, [Triz]Cl/DETA demonstrated both the highest cyclic loading and the highest desorption efficiency, highlighting its potential as a highly regenerable absorbent. Notably, although [Triz]Cl/EDA exhibited a higher cyclic

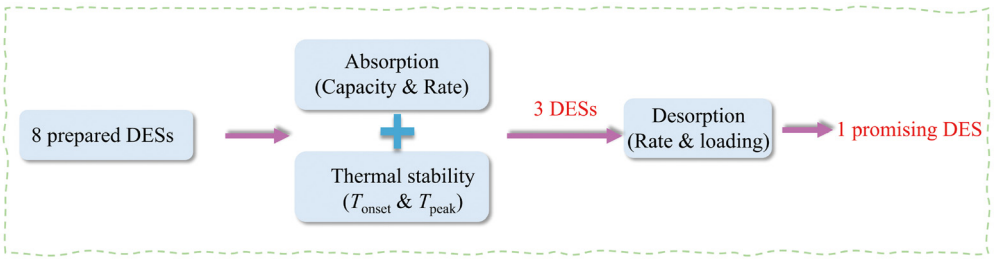

Fig. 4 Stepwise methodology adopted for the screening of DESs.

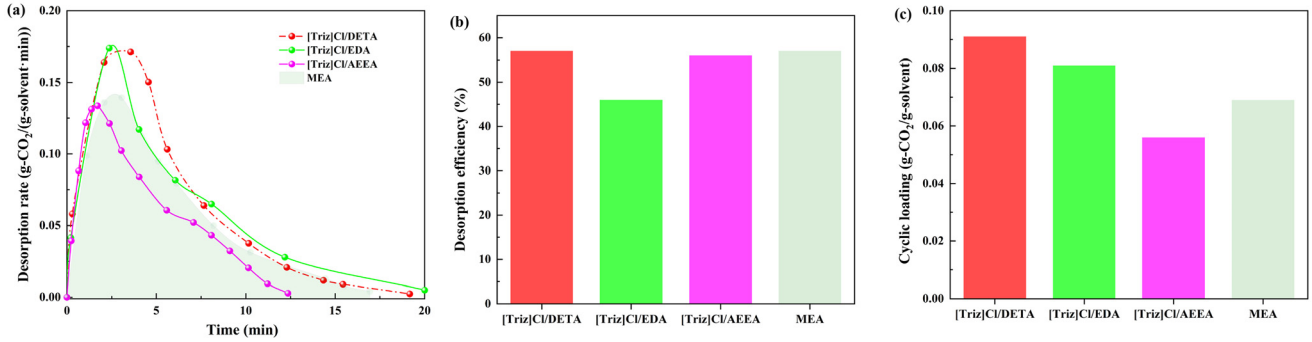

Fig. 5 (a) CO_2 desorption curves, (b) desorption efficiencies, and (c) CO_2 cyclic loading of aqueous DESs and MEA.

loading than MEA, it showed the lowest desorption efficiency. This may be attributed to the stronger CO_2 binding affinity of EDA, which impedes complete desorption under moderate thermal conditions.

3.5. Global comparison and second-step screening

Based on a comprehensive evaluation of key performance metrics, including CO_2 absorption capacity, apparent rate constant, thermal stability, desorption efficiency, and cyclic loading, as shown in Table 5, the 30 wt% [Triz]Cl/DETA aqueous solution was identified as the most promising absorbent. It exhibits high absorption performance (n_t = 0.17 g-CO_2 per g-solvent, K_a = 0.18 min^{-1}), outstanding thermal stability (T_{onset} = 178 °C with only 0.7% weight loss at 110 °C), and the highest cyclic CO_2 loading (0.09 g-CO_2 per g-solvent), while maintaining a desorption efficiency comparable to that of MEA.

To further integrate and compare the multiple performance indicators of DESs, a radar chart was constructed using normalized data, as shown in Fig. 6. All performance metrics were normalized to a 0–1 range using Min–Max scaling methods (eqn (S1) in the SI), with weight loss converted to residual mass. This comprehensive visualization enables a direct comparison of overall performance across different systems. Based on this analysis, the 30 wt% [Triz]Cl/DETA aqueous solution was also identified as the most promising absorbent (Fig. 4).

3.6. Further research on [TrizCl][DETA]

3.6.1. Viscosity before and after CO_2 absorption. The viscosity of the 30 wt% [Triz]Cl/DETA aqueous solution was measured before and after CO_2 absorption and compared with that of 30 wt% MEA aqueous solution, as shown in Fig. 7.

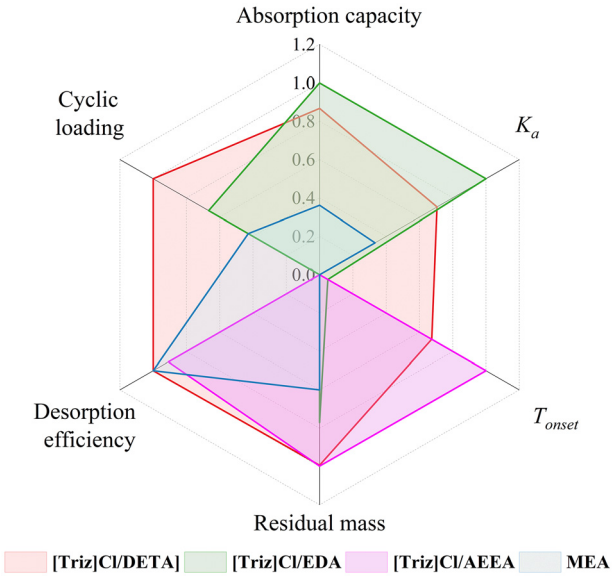

Fig. 6 Comprehensive performance comparison of CO_2 absorbents.

Upon CO_2 absorption, the viscosity of [Triz]Cl/DETA increased due to the formation of carbamate species, which enhanced hydrogen bonding and ionic interactions and thus restricted molecular mobility. The effect was more pronounced than in MEA because the polyamine structure of [Triz]Cl/DETA provides multiple reactive sites that facilitate the formation of denser hydrogen-bonding networks. Nevertheless, the viscosity of the [Triz]Cl/DETA solution after CO_2 absorption remained below 7 mPa s, which is sufficiently low for CO_2 capture.

3.6.2. Oxidative stability test. To evaluate the oxidative stability of the aqueous DES under practical conditions, its

Table 5 Comprehensive performance comparison of DESs

Absorbent	Absorption capacity n_t (g-CO_2 per g-solvent)	Apparent rate constant K_a (min^{-1})	T_{onset} (°C)	Weight loss at 110 °C (%)	Desorption efficiency η (%)	Cyclic loading n_c (g-CO_2 per g-solvent)
[Triz]Cl/DETA	0.17	0.18	178	0.7	57%	0.09
[Triz]Cl/EDA	0.18	0.20	90	23	46%	0.08
[Triz]Cl/AEEA	0.09	0.15	224	0.2	56%	0.05
MEA	0.12	0.16	83	40	57%	0.07

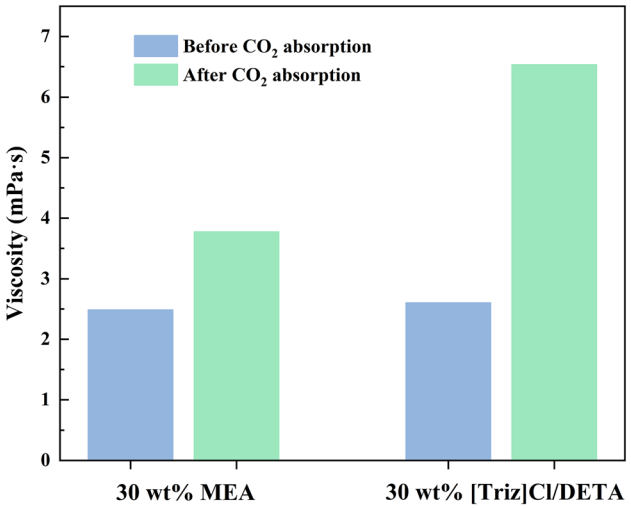

Fig. 7 Viscosity of 30 wt% [Triz]Cl/DETA and MEA aqueous solutions before and after CO_2 absorption.

potential reactivity toward common industrial gas components, N_2 and O_2, was examined. The 30 wt% [Triz]Cl/DETA aqueous solution was maintained at 22 °C and continuously purged with either N_2 or O_2 for 5 hours; the samples were then analyzed by FTIR, and the spectra were compared with those of the fresh sample. As shown in Fig. 8, no noticeable variations were observed in the characteristic absorption bands after exposure to either gas, indicating that the chemical composition and molecular structure of the DES remained unchanged. Furthermore, to simulate desorption conditions, the solvent was exposed to O_2 at 110 °C for 5 hours, followed by FTIR analysis (Fig. 8). No new peaks or significant intensity

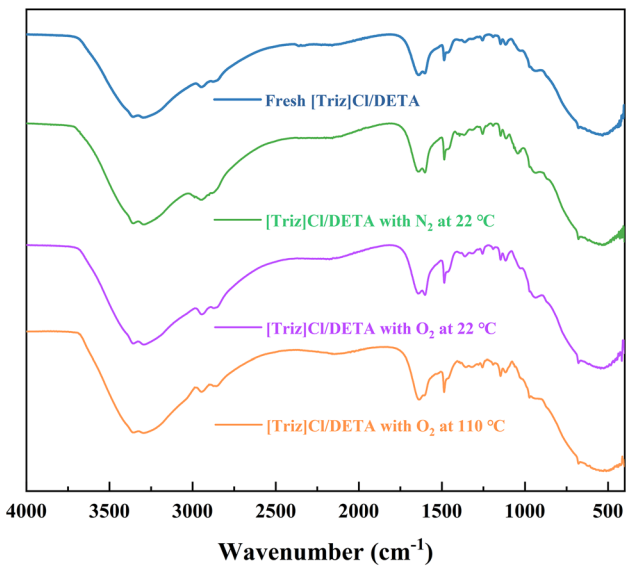

Fig. 8 FTIR spectra of 30 wt% [Triz]Cl/DETA aqueous solutions: fresh, after 5 h exposure to N_2 or O_2 at 22 °C, and after 5 h exposure to O_2 at 110 °C.

changes were detected, confirming that aqueous [Triz]Cl/DETA exhibits excellent oxidative stability even at 110 °C. These findings demonstrate the excellent oxidative stability of aqueous [Triz]Cl/DETA, suggesting its suitability for long-term gas treatment applications without oxidative degradation.

3.6.3. Corrosion analysis. Considering the critical influence of corrosion on the industrial applicability of CO_2 capture solvents, the corrosion behavior of 20# carbon steel was tested in both conventional 30 wt% MEA and the novel 30 wt% [Triz]Cl/DETA aqueous solutions at room temperature. The corrosion rates were obtained from the Tafel polarization measurements, as illustrated in Fig. 9(a). In the CO_2-free state, the [Triz]Cl/DETA solution exhibited a substantially lower corrosion rate than MEA, measured at 1.2×10^{-4} and 2.3×10^{-4} mm a^{-1}, respectively (Fig. 9(b)). Upon CO_2 loading, the corrosion rates of both systems increased; however, the rise was considerably less pronounced for [Triz]Cl/DETA. Specifically, its corrosion rate increased to 7.5×10^{-4} mm a^{-1}, whereas that of MEA reached 1.8×10^{-3} mm a^{-1}. These results clearly indicate that the aqueous [Triz]Cl/DETA system possesses higher corrosion resistance and is significantly less susceptible to CO_2-induced corrosion than the conventional aqueous MEA.

3.6.4. The role of HBA and HBD in [Triz]Cl/DETA. To elucidate the CO_2 absorption mechanism of aqueous [Triz]Cl/DETA (30 wt% DES + 70 wt% H_2O), both FTIR and ^{13}C NMR analyses were conducted before and after CO_2 absorption. As shown in Fig. 10(a), the emergence of new peaks at 1546 and 819 cm^{-1} in the FTIR spectra can be attributed to C═O and C–O stretching vibrations, respectively, which are indicative of carbamate formation. Peaks at 1090 and 1162 cm^{-1} were assigned to C–N and symmetric C–O stretching,[36] while a shoulder near 1327 cm^{-1} reflected the characteristic vibration of carbamate C═O groups.[11]

In parallel, Fig. 10(b) shows the ^{13}C NMR spectra of [Triz]Cl/DETA before and after CO_2 absorption. A new peak at ~165 ppm appeared in the ^{13}C NMR spectrum of CO_2-loaded [Triz]Cl/DETA, which was attributed to the carbonyl carbon of the carbamate species (–NHCOO–), confirming that chemical absorption occurred *via* the formation of zwitterionic intermediates, followed by stabilization through proton transfer. New signals were observed near 48 ppm, corresponding to the $–CH_2–N–$ groups formed after the CO_2 absorption. Moreover, a slight upfield shift near 45 ppm indicates changes in the local electronic environment of the amine carbon atoms, reflecting hydrogen-bond rearrangement and proton exchange during carbamate formation.[37] These observations collectively support the reaction of amine sites with CO_2.[38]

To further clarify which component interacts with CO_2 and how the DES structure is formed, the FTIR spectra of 30 wt% DETA, 30 wt% [Triz]Cl, and 30 wt% [Triz]Cl/DETA were compared (Fig. S6). New bands at 2361 and 1255 cm^{-1} appear only for 30 wt% [Triz]Cl/DETA, indicating specific hydrogen-bond interactions between the HBA ([Triz]Cl) and HBD (DETA). After CO_2 absorption, 30 wt% [Triz]Cl shows only minor spectral changes, whereas 30 wt% DETA clearly displays new carbamate bands, and the CO_2-loaded spectrum of 30 wt% [Triz]Cl/DETA

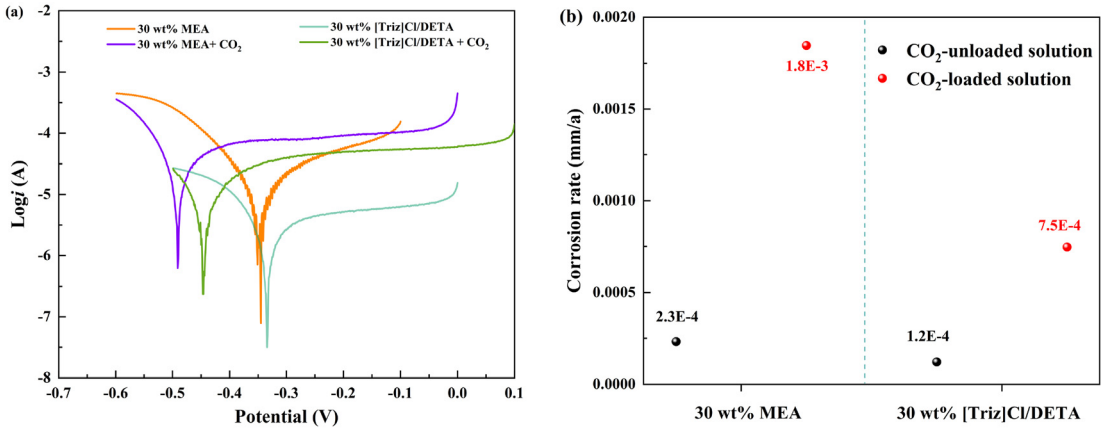

Fig. 9 (a) Tafel polarization curves of carbon steel in 30 wt% MEA and [Triz]Cl/DETA aqueous solutions; (b) corresponding corrosion rates determined from the Tafel extrapolation.

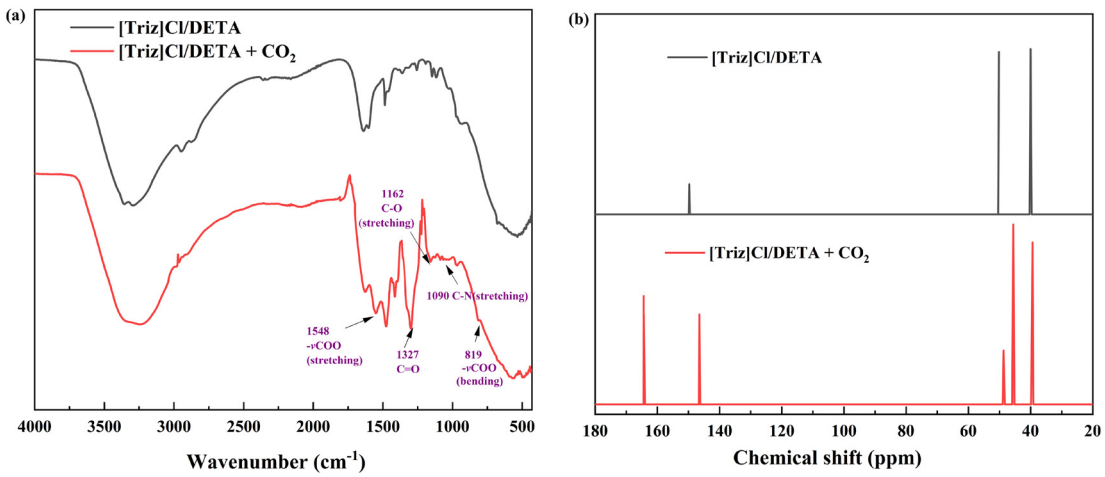

Fig. 10 (a) FTIR and (b) ^{13}C NMR spectra of [Triz]Cl/DETA before and after CO_2 absorption.

closely matches that of CO_2-loaded DETA. These results confirm that DETA provides the chemically active –NH– sites for CO_2 binding, while [Triz]Cl mainly acts as the hydrogen-bond acceptor matrix rather than reacting directly with CO_2.

The respective roles of [Triz]Cl and DETA are also reflected in the macroscopic CO_2 absorption behaviour and thermal stability. As shown in Fig. S7 (SI), 30 wt% DETA shows the highest CO_2 capacity (0.20 g-CO_2 per g-solvent) but a slower absorption rate than 30 wt% [Triz]Cl/DETA, whereas 30 wt% [Triz]Cl exhibits only a very low CO_2 capacity (0.02 g-CO_2 per g-solvent). In 30 wt% [Triz]Cl/DETA, the DETA content is 24.9 wt%. For comparison, the CO_2 absorption capacity of 24.9 wt% DETA was estimated, proving a value of 0.16 g-CO_2 per g-solvent, which is almost the same as that of 30 wt% [Triz]Cl/DETA (0.17 g-CO_2 per g-solvent). Therefore, DETA provides the main chemically active –NH– sites for CO_2 binding. The thermal stabilities of pure DETA and [Triz]Cl were also measured under the same conditions for comparison (Fig. 3). Both the T_{onset} and T_{peak} values of DETA are lower than those of [Triz]Cl/DETA, whereas [Triz]Cl shows higher T_{onset} and T_{peak} values than both DETA and [Triz]Cl/DETA. These observations confirm that [Triz]Cl does not significantly absorb CO_2 and primarily acts as a hydrogen-bond acceptor framework, thereby improving the physicochemical properties of the DES (*e.g.*, thermal stability).

3.6.5. Sensible heat requirement for solvent regeneration. A simplified metric was introduced to compare the sensible heat requirement during the [Triz]Cl/DETA regeneration. Briefly, the sensible heat required to raise the solvent from the absorption temperature (22 °C) to the desorption temperature (110 °C) was estimated, which was then normalized by the cyclic CO_2 loading to obtain an indicative sensible heat requirement per unit CO_2. The detailed calculation procedure is provided in the SI (section 2). Based on this simplified analysis and assuming a specific heat capacity like that of typical aqueous amine solutions, the simplified sensible-heat index for 30 wt% [Triz]Cl/DETA is about 25% lower than that for 30 wt% MEA. Combined with the much lower mass loss at

110 °C (0.7% *vs.* 40%), these results indicate that [Triz]Cl/DETA is intrinsically favorable for energy-efficient regeneration.

It should be noted that this simplified metric reflects only the sensible-heat contribution. Indeed, the energy demand for solvent regeneration is a joint contribution of sensible heat to increase temperature, CO_2 absorption enthalpy, and energy used for vaporization. This work focused on the screening of effective solvents. Once the effective solvents are identified, in our future work, equilibrium and calorimetric measurements together with process-level simulations will be carried out to quantify the overall regeneration energy of the promising DES systems.

4. Conclusions

In this study, a series of DESs were synthesized using [Triz]Cl as the HBA and eight different amine-based compounds as HBDs to evaluate the relationship between HBD structure and CO_2 capture performance. The results demonstrated that the molecular structure and functionality of the HBD significantly influenced the CO_2 absorption capacity, absorption rate, thermal stability, and desorption performance. Specifically, short-chain polyamines such as EDA and DETA exhibited high CO_2 absorption capacities (0.18 and 0.17 g-CO_2 per g-solvent, respectively) owing to their dense –NH– active sites that facilitate carbamate formation; the thermal stability of the DESs follows the trend [Triz]Cl/TEPA > [Triz]Cl/AEEA > [Triz]Cl/MDEA > [Triz]Cl/DETA > [Triz]Cl/DEA > [Triz]Cl/AMP > [Triz]Cl/MEA > [Triz]Cl/EDA, emphasizing that stronger hydrogen-bond networks and higher molecular weights of the HBD enhance resistance to decomposition. Among them, 30 wt% [Triz]Cl/DETA exhibited the highest cyclic CO_2 loading (0.09 g-CO_2 per g-solvent) and desorption efficiency (57%), coupled with superior oxidative and corrosion stability, confirming its industrial applicability. FTIR and ^{13}C NMR analyses confirmed the formation of the carbamate species, providing clear evidence of chemical absorption of CO_2 in the [Triz]Cl/DETA systems. Overall, this work establishes clear structure–property correlations for DES-based CO_2 absorbents, demonstrating that optimizing amine density, molecular flexibility, and hydrogen-bonding interactions is key to balancing absorption performance, regeneration efficiency, and stability. These features suggest that the 30 wt% [Triz]Cl/DETA aqueous solution is a more energy-efficient and equipment-friendly CO_2 absorbent than the 30 wt% MEA aqueous solution, offering a clear green chemistry advantage.

Author contributions

Qiangbing Shi: data curation and writing – original draft. Kaige Jia: writing – original draft. Xiangping Zhang: methodology and validation. Chuan Wang: validation. Paul Cobden: validation. Anna-Maria Beregi Amnéus: validation. David Muren: validation. Xiaoyan Ji: validation, conceptualization, supervision, and funding acquisition.

Conflicts of interest

The authors declare that they have no known competing financial interests or personal relationships that could have appeared to influence the work reported in this paper.

Data availability

The data supporting this article have been included as part of the supplementary information (SI). Supplementary information is available. Supplementary information: a schematic diagram of the CO_2 absorption and desorption apparatus, TG and DTG curves, CO_2 desorption behavior at different temperatures, and details of the min-max scaling method. See DOI: https://doi.org/10.1039/d5gc05611j.

Acknowledgements

This work was financially supported by the Swedish Energy Agency (Energimyndigheten) (P2021-00004), the European Union, STINT (CH2019-8287), and the National Key Research and Development Program of China (2024YFE0206200).

References

1 H. C. Lau and S. C. Tsai, *Energies*, 2023, **16**, 7800.
2 I. E. Agency, *Global Energy Review 2025*, Paris, 2025.
3 H. Wu, Q. Li, M. Sheng, Z. Wang, S. Zhao, J. Wang, S. Mao, D. Wang, B. Guo, N. Ye, G. Kang, M. Li and Y. Cao, *J. Membr. Sci.*, 2021, **624**, 119137.
4 A. G. Olabi and M. A. Abdelkareem, *Renewable Sustainable Energy Rev.*, 2022, **158**, 112111.
5 D. Garza, P. Dargusch and D. Wadley, *Energies*, 2023, **16**, 4090.
6 I. M. Bernhardsen and H. K. Knuutila, *Int. J. Greenhouse Gas Control*, 2017, **61**, 27–48.
7 G. Cui, J. Wang and S. Zhang, *Chem. Soc. Rev.*, 2016, **45**, 4307–4339.
8 D. O. Abranches and J. A. P. Coutinho, *Annu. Rev. Chem. Biomol. Eng.*, 2023, **14**, 141–163.
9 J. Ju, D. Choi, S. Cho, Y. Yoo and D. Kang, *Chem. Eng. J.*, 2024, **496**, 153922.
10 B. Jiang, J. Ma, N. Yang, Z. Huang, N. Zhang, X. Tantai, Y. Sun and L. Zhang, *Energy Fuels*, 2019, **33**, 7569–7577.
11 T. J. Trivedi, J. H. Lee, H. J. Lee, Y. K. Jeong and J. W. Choi, *Green Chem.*, 2016, **18**, 2834–2842.
12 S. Imteyaz and P. P. Ingole, *J. Mol. Liq.*, 2023, **376**, 121436.
13 B. Lu, Y. Zeng, M. Chen, S. Zhang and D. Yang, *Atmosphere*, 2024, **15**, 229.
14 Q. Shi, K. Jia, X. Zhang, C. Wang, P. Cobden, A.-M. B. Amnéus, D. Muren and X. Ji, *Chem. Eng. J.*, 2025, **522**, 167866.
15 F. Gabriele, M. Chiarini, R. Germani, M. Tiecco and N. Spreti, *J. Mol. Liq.*, 2019, **291**, 111301.
16 K. G. Jia, Q. B. Shi and X. Y. Ji, *Green Chem. Eng.*, 2025, **6**, 562–571.

17 N. Ahmad, X. Lin, X. Wang, J. Xu and X. Xu, *Fuel*, 2021, **293**, 120466.
18 S. Foorginezhad and X. Ji, *Sep. Purif. Technol.*, 2024, **347**, 127593.
19 M. Yan, Q. Huan, Y. Zhang, W. Fang, F. Chen, A. Pariatamby, E. Kanchanatip and H. Wibowo, *Biomass Convers. Biorefin.*, 2024, **14**, 283–297.
20 S. Foorginezhad and X. Ji, *Carbon Capture Sci. Technol.*, 2025, **15**, 100385.
21 L. Xiao, Z. Qiu, S. Feng, X. Duan, Z. Zhao, Y. Liu and L. Ma, *Chem. Eng. Process.*, 2024, **204**, 109931.
22 E. I. Ahmed, K. S. Ryder and A. P. Abbott, *Electrochim. Acta*, 2021, **397**, 139284.
23 X. Li, M. Hou, B. Han, X. Wang and L. Zou, *J. Chem. Eng. Data*, 2008, **53**, 548–550.
24 S. Sarmad, J. P. Mikkola and X. Ji, *ChemSusChem*, 2017, **10**, 324–352.
25 K. Zhang, Y. Hou, Y. Wang, K. Wang, S. Ren and W. Wu, *Energy Fuels*, 2018, **32**, 7727–7733.
26 G. Cui, M. Lv and D. Yang, *Chem. Commun.*, 2019, **55**, 1426–1429.
27 S. Sarmad, Y. Xie, J.-P. Mikkola and X. Ji, *New J. Chem.*, 2017, **41**, 290–301.
28 L. F. Zubeir, D. J. G. P. van Osch, M. A. A. Rocha, F. Banat and M. C. Kroon, *J. Chem. Eng. Data*, 2018, **63**, 913–919.
29 S. K. Shukla and J.-P. Mikkola, *Chem. Commun.*, 2019, **55**, 3939–3942.
30 X. Song, J. Yuan, C. Yang, G. Deng, Z. Wang and J. Gao, *Renewable Sustainable Energy Rev.*, 2023, **184**, 113499.
31 S. Sarmad, J.-P. Mikkola and X. Ji, *ChemSusChem*, 2017, **10**, 324–352.
32 S. K. Shukla, Y. L. Wang, A. Laaksonen and X. Ji, *Chem. Commun.*, 2023, **59**, 10516–10519.
33 F. Meng, T. Ju, S. Han, L. Lin, J. Li, K. Chen and J. Jiang, *Sep. Purif. Technol.*, 2023, **310**, 123195.
34 Y. G. Ko, S. S. Shin and U. S. Choi, *J. Colloid Interface Sci.*, 2011, **361**, 594–602.
35 J. T. Cullinane and G. T. Rochelle, *Ind. Eng. Chem. Res.*, 2006, **45**, 2531–2545.
36 S. F. R. Taylor, M. McClung, C. McReynolds, H. Daly, A. J. Greer, J. Jacquemin and C. Hardacre, *Ind. Eng. Chem. Res.*, 2018, **57**, 17033–17042.
37 X. Sun, S. Zeng, G. Li, Y. Bai, M. Shang, J. Zhang and X. Zhang, *AIChE J.*, 2024, **70**, e18376.
38 X. Zhan, B. Lv, K. Yang, G. Jing and Z. Zhou, *Environ. Sci. Technol.*, 2020, **54**, 6281–6288.